Aromatic−Backbone Interactions in α-Helices

Gergely Tóth,[†,‡] Katalin E. Kövér,[§] Richard F. Murphy,[†] and Sándor Lovas*[,†]

Department of Biomedical Sciences, Creighton University, Omaha, Nebraska 68178, and Department of Inorganic and Analytical Chemistry, University of Debrecen, H-4010, Debrecen, Egyetem tér 1, P.O. Box 21, Hungary

Received: December 19, 2003; In Final Form: April 1, 2004

The interaction between the aromatic ring of an amino acid and the α-helical polypeptide backbone was investigated by studying the conformation of α-helical Ala-based model peptides, with Tyr replacement in the N-terminal and inner helical positions, using ^{1}H NMR, molecular dynamics (MD) simulations, and a protein database search. NOE cross-peaks between the hydrogens of the aromatic ring at position *i* and the hydrogen of the backbone amide in positions *i*, *i*+1, *i*+3 and *i*+4 indicated the proximity of the aromatic ring to the backbone. Interaction between the aromatic ring and the backbone seemed to be highly dependent on the orientation of the aromatic side chain to the helical backbone because aromatic−backbone amide, aromatic−carbonyl, and aromatic−HCα interactions were observed in MD. Solvent screening by the aromatic side chain decreased the solvent accessible surface area of some polar backbone groups by more than 80%. These results indicate that aromatic−backbone interactions commonly occur in helical structures in proteins.

Introduction

The delicate balance of noncovalent interactions determines the three-dimensional structure of peptides and proteins. These interactions include hydrogen bonds, salt bridges, weakly polar interactions,[1] and the hydrophobic effect. Weakly polar interactions[2] can occur between aromatic side chains of amino acids and groups with hydrogen bond donating potential. Aromatic rings in polypeptides can interact with ions, for example, in aromatic−cation interactions,[3] with dipoles,[1,4,5] for example, in aromatic−backbone amide (Ar−HN) interactions,[6−8] and with quadrupoles, for example, in aromatic−aromatic interactions.[9,10] The strength of these noncovalent interactions varies depending on the nature of the interacting partner group.[11]

Some weakly polar interactions in α-helices have been investigated. For example, interactions between the side chains of aromatic amino acids and (1) side chains of Arg and Lys in *i*, *i*+4 pairs,[12−14] (2) the hydrophobic side chains of Leu, Ile, Val, Cys, Met, in *i*, *i*+3, *i*, *i*+4, *i*, and *i*+5 pairs,[15,16] and (3) the aromatic side chain of Phe-His and Trp-His, in *i*, *i*+4 pairs.[17−19] All these interactions were found to stabilize the α-helical structure in polypeptides.

Side chain−backbone interactions in α-helices have also been investigated. For example, the side chains of Thr, Ser, Asp, and Asn form hydrogen bonds with neighboring backbone amides in α-helices. These side chains compete with the backbone carbonyl group for hydrogen bonding with the backbone amide and thus, tend to break backbone carbonyl-amide hydrogen bonds. Therefore, in the N-cap and N-terminal positions of the α-helix, side chain−backbone interactions are considered to stabilize and nucleate the α-helix, whereas in the inner and C-terminal positions of the helix this interaction has the opposite effect.[20] Previous work in this and other laboratories[8,21] found that aromatic rings interact with neighboring backbone amides in α-helices in proteins.

TABLE 1: NMR Analyses of Peptides Y0−Y6[a]

	amino acid sequence	$FH^{NMR}_{^3J_{HN\alpha}}$	$FH^{NMR}_{\alpha CH}$
Y0	Ac-AAAAAAAEAAKA-NH2	0.57	0.65
Y1	Ac-YAAAAAAEAAKA-NH2	0.53	1.48
Y2	Ac-AYAAAAAEAAKA-NH2	0.47	0.65
Y3	Ac-AAYAAAAEAAKA-NH2	0.58	0.57
Y4	Ac-AAAYAAAEAAKA-NH2	0.58	0.86
Y5	Ac-AAAAYAAEAAKA-NH2	0.23	0.75
Y6	Ac-AAAAAYAEAAKA-NH2	0.23	0.63

[a] Fractional helical content ($FH^{NMR}_{^3J_{HN\alpha}}$, $FH^{NMR}_{\alpha CH}$) was calculated from NMR data using the method described by Lacroix and co-workers.[35] $FH^{NMR}_{^3J_{HN\alpha}}$, $FH^{NMR}_{\alpha CH}$ were calculated on the basis of $^3J_{HN\alpha}$ and chemical shifts of αCH.

In this study, the interaction between the aromatic side chain of Tyr and the helical backbone was investigated by studing Ala-based α-helical model peptides using ^{1}H NMR spectroscopy and molecular dynamics (MD). A complex network of weakly polar interactions between the aromatic ring and the helical backbone was found on the basis of the NMR and MD results. Further investigation of these interactions in α-helices of proteins in the Protein Data Bank[22] confirmed that this observation is a common phenomenon in proteins. In light of these findings, the solvation of the helical polar backbone and the effect of these interactions on the α-helix stability is discussed.

Materials and Methods

Design of Ala-Based α-Helical Model Peptides. The stability of the α-helical conformation of model peptides should be derived from the properties of the polypeptide backbone itself; thus, the likelihood of interactions between side-chains of the substituted residue and of other residues in the sequence was avoided as much as possible. The template peptide, **Y0**, was mostly composed of Ala (Table 1). To increase solubility in water, Glu was inserted in the inner helix at position 8 and Lys was placed in the C-terminal position 11. The charged side

* Corresponding author. Phone: 402-280-5753. Fax: 402-280-2690. E-mail: slovas@bif1.creighton.edu.
† Creighton University.
‡ Present address: Protein Mechanics Inc., Mountain View, CA.
§ University of Debrecen.

10.1021/jp037945y CCC: $27.50
Published on Web 05/14/2004

chains of two residues can form an *i*, *i*+3 ion bridge, which has a stabilizing effect on the helical structure of the peptide.[23] Lys in the C-terminal region could further stabilize the helical structure of the host peptide because its positively charged side chain can interact with the macrodipole of the α-helix.[24] Model peptides (Table 1) were generated by replacing Ala in positions 1−6 with Tyr. Tyr was chosen as the aromatic residue, because it is more hydrophilic than Phe or Trp.

Peptide Synthesis. Peptides were synthesized by Fmoc (9-fluorenylmethoxycarbonyl) chemistry at a 0.025 mM scale on a polystyrene-based resin with Knorr linker[25] using HBTU/HOBt (2-(1*H*-benzotriazol-1-yl)-1,1,3,3-tetramethyluronium hexafluorophosphate/1-hydroxybenzotriazole) as coupling reagents and an ABI 423A automated peptide synthesizer. *tert*-Butyl protection was used for the side chains of Tyr and Glu and *tert*-butyloxycarbonyl group for the side chain of Lys. The N-terminal α-amino groups of the completed peptides were acetylated using a mixture of acetic anhydride, diisopropyl-ethylamine and *N*,*N*-dimethyl formamide (2:1:17, v/v/v). Peptides were cleaved from the resin with a mixture of trifluoroacetic acid, thioanisole, and ethanedithiol (18:1:1, v/v/v). Crude peptides were purified by reversed-phase HPLC on a Vydac C_{18} column (5 μm particle size) using a gradient of acetonitrile containing 0.09% trifluoroacetic acid in water contining 0.1% trifluoroacetic acid. Purified peptides were identified by electrospray mass spectrometry (observed mass of **Y0** 1027.6 Da, calculated mass of **Y0** 1026.6 Da; observed mass of **Y1** 1119.6 Da, calculated mass of **Y1** 1118.6 Da; observed mass of **Y2** 1119.6 Da, calculated mass of **Y2** 1118.6 Da; observed mass of **Y3** 1119.8 Da, calculated mass of **Y3** 1118.6 Da; observed mass of **Y4** 1120.0 Da, calculated mass of **Y4** 1118.6 Da; observed mass of **Y5** 1120.0 Da, calculated mass of **Y5** 1118.6 Da; observed mass of **Y6** 1120.0 Da, calculated mass of **Y6** 1118.6 Da).

NMR Measurements. D_2O (1 vol) was added to 2−3 mM peptide solutions (9 vol) in 0.1 M NaCl, 0.1 mM Na_2HPO_4. Any resultant peptide precipitate was removed by filtration.

All NMR measurements were carried out on a Bruker Avance DRX 500 NMR spectrometer with an operating frequency of 500.13 MHz for protons at 275 K. Chemical shifts were referenced to measurements for sodium 3-trimethylsilyl-(2,2,3,3-$^2H_4$) propionate at 0.00 ppm. Gradient-enhanced, pure absorption phase 2D TOCSY[26,27] spectra were recorded with 62 ms MLEV-17 spin-locking pulse. Gradient-enhanced NOESY with water flip-back pulse[28,29] was employed to record the NOESY spectra with a mixing time of 150 ms. Proton chemical shifts and homonuclear coupling constants were extracted from resolution enhanced 1D proton and/or pure phase 2D TOCSY spectra.

Sequential assignment of proton resonances was obtained using the homonuclear 2D TOCSY and NOESY spectra, as previously proposed by Wüthrich.[30] NOESY spectra were used to infer the interresidue dipolar (through space) connectivities. Amide temperature coefficients were obtained from 1D proton and/or 2D TOCSY spectra recorded at 275, 280, and 285K.

The helical nature of the peptides were determined using αCH−HN proton−proton spin−spin coupling constants,[31] $^3J_{HN\alpha}$ upfield shifts of αCH proton resonances relative to random coil values,[32] amide proton temperature coefficients,[33,34] and a set of characteristic NOEs.[33]

The fractional helical content of the peptides was calculated from NMR data (FH^{NMR}) using the method of Lacroix and coworkers.[35] $FH^{NMR}_{\delta_{\alpha CH}}$ was calculated from αCH proton chemical shifts, $\delta_{\alpha CH}$. The values of $\delta_{\alpha CH}$ in 100% helical structure were those of Wisthart and associates;[36] 0.1 ppm was added to these values due to the higher flexility of peptides than of proteins. Random coil values of $\delta_{\alpha CH}$ were those of Wishart and associates.[32] The effect of the aromatic ring on $\delta_{\alpha CH}$ was not included in the calculations. Calculation of $FH^{NMR}_{^3J_{HN\alpha}}$ was based on $^3J_{HN\alpha}$ coupling constants; 4.2 Hz was used as the value of the $^3J_{HN\alpha}$ coupling constant for 100% helical structure. Calculation of the random coil values of the $^3J_{HN\alpha}$ coupling constant was based on the Boltzmann distribution.[38]

Molecular Dynamics (MD) Simulations. All molecular dynamics calculations were done using the modified GROMOS-87 force field as implemented in the GROMACS 2.0 program package[38] The starting structures of the peptides, created with Sybyl 6.2,[39] were α-helical, and the χ^1 torsion angle of Tyr was set to 180°. Each starting structure was immersed in a cubic box (36 Å × 36 Å × 36 Å) of SPC/E water molecules so that all water molecules with oxygen atoms less than 2.8 Å or hydrogen atoms less than 2.0 Å from the peptide were removed. All systems were energy minimized using the steepest descent method until the difference between the total potential energies of the molecular system at consecutive energy minimization steps was less than 0.001 kJ mol^{-1}. Then, NVT MD was performed for 20 ps by positionally restraining the peptide in the center of the box with a force of 1000 kJ mol^{-1} at 300 K, to allow the solvent density to approach the equilibrium value. A total of 20 100 ps MD trajectories at a constant temperature of 300 K and constant pressure of 1 atm were generated. The first 100 ps was regarded as the equilibration period and was excluded from the trajectory analysis. The parameters of the molecular dynamics simulations were as follows: 2 fs steps; LINCS algorithm[40] used to set bonds to their correct length with the warning angle of 30°; nonbonded interactions list updated every 10 steps; reaction field method with cutoff distances of 1.4 and 1.3 nm for Coulomb and van der Waals interactions, respectively; 78 as the constant dielectric beyond 1.4 nm; the peptide and solvent coupled to separate temperature baths with a relaxation constant of 0.1 ps; the peptide and solvent coupled to a pressure bath using isotropic and atomic scaling with a relaxation constant of 0.5 ps. The coordinates of the peptide were stored for evaluation every 1000 steps to yield a total of 10 050 sampled conformations for each trajectory.

The energy of the interaction between the aromatic ring of Tyr and the backbone, in selected α-helical structures of **Y1**−**Y6** from the MD, was calculated using the same force field as above with the g_energy program from the analysis suite of GROMACS 2.0. Selected structures from the trajectories were energy minimized using the steepest descent algorithm. The dielectric constant was set to 78. The minimization was stopped either when the gradient was smaller than 0.001 kJ mol^{-1} nm^{-1} or after 1000 steps. The maximum initial step-size was 0.005 nm. For the same interaction energy calculations, structures from the PDB were not energy minimized.

The trajectories were analyzed using the analyses suite of GROMACS 2.0 to determine total energy, torsion angles, and secondary structure. The secondary structure of the peptides in each trajectory was determined using the DSSP program.[41] For further analyses, structures from each trajectory with residues 2−10 in α-helical conformation, were selected on the basis of DSSP output and referred to as selected α-helical structures. The solvent accessible surface area (SASA) of the peptides, the backbone amides and the side chain phenolic group of Tyr was calculated with the NACESS program.[42]

The Ar−HN and π−HC interactions were assigned on the basis of backbone amide and H−C hydrogen NMR ring shift (δ_{ring}). δ_{ring} is the shift in the value of the chemical shift (δ)

TABLE 2: Protein Fragments with Residues in α-Helical (H) and Non-α-Helical (X) Conformation Sought with the Sybyl Script #1[a]

position	protein fragment
N_{cap}	−**X**−H−H−H−H−
N1	−X−**H**−H−H−H−H−
N2	−X−H−**H**−H−H−H−H−
N3	−X−H−H−**H**−H−H−H−H−
N4−C4	−H−H−H−H−H−H−H−**H**−H−H−H−H−H−H−H−
C3	−H−H−H−H−**H**−H−H−X−
C2	−H−H−H−H−**H**−H−X−
C1	−H−H−H−H−**H**−X−
C_{cap}	−H−H−H−H−**X**−

[a] Characters in bold show the position of either Phe, Tyr, or Trp.

due to the change in the local magnetic field of the proton resulting from the nearby delocalized electrons of an aromatic ring during the ^{1}H NMR experiments. The value of δ_{ring} is influenced by the geometry of the Ar—HN interaction.[6,8] An Ar—NH and π—HC interaction was assigned when the value of backbone amide hydrogen δ_{ring} was −0.5 ppm or lower[6,43,44] and the value of the H—C hydrogen δ_{ring} was −0.25 or lower.[46,44] The Total program[47] was used to calculate the hydrogen δ_{ring}. The interaction between C—H of the aromatic rings and backbone carbonyl groups (Ar—CO) was detected when the distance between the hydrogen of the C—H group and the oxygen of the C═O group was less than 3.0 Å, the distance between the carbon of the C—H group and the oxygen of the C═O group was less than 3.8 Å and when the angle C—H···O was greater than 95°.[48]

The nonhomologous protein database of SYBYL 6.3[39] was searched using SYBYL script #1 for fragments with α-helical structure. Table 2 shows the polypeptide fragments sought. Selected coordinate files of the protein fragments were stored in SYBYL databases. SYBYL script #2 was used to calculate χ^1 and χ^2 torsion angles of Tyr, Phe, and Trp in the fragments. Torsion angle χ^1 was classified as followins: trans (*t*) 180° ± 60°, gauche+ (*g*+) 60° ± 60°, gauche− (*g*−) −60° ± 60°.

Results

NMR Measurements. The HN1−HN4 and most of the HN8−HN12 amide protons were resolved. The chemical shifts of the HN and αCH hydrogens (δ_{HN} and $\delta_{\alpha CH}$) are listed in the Supporting Information. The possible effect of the aromatic ring on δ_{HN} and $\delta_{\alpha CH}$ could be estimated from the difference ($\Delta\delta_{HN}$ and $\Delta\delta_{\alpha CH}$ in Table 2 of Supporting Information) between δ_{HN} and $\delta_{\alpha CH}$ of a residue in **Y0** and δ_{HN} and $\delta_{\alpha CH}$ of the same residue in the selected peptide, provided the secondary structure was the same for all peptides. Upfield shifts of δ_{HN} were observed in positions *i* and *i*+1 in **Y1** and in position *i*+1 in **Y2** and **Y3**. $FH^{NMR}_{\delta_{\alpha CH}}$ values (Table 1) indicating that **Y1**, **Y4**, and **Y5** are more helical than **Y0**, whereas **Y2**, **Y3**, and **Y6** are approximately as helical as **Y0**.

The $^3J_{HN\alpha}$ coupling constant is related to torsion angle ϕ,[49] and thus, from the $^3J_{HN\alpha}$ coupling constants of subsequent residues, the secondary structure of a polypeptide chain can be deduced. The $^3J_{HN\alpha}$ coupling constants, calculated from a database of high-resolution crystal structures of proteins[31] are 4.8, 5.6, and 8.5 Hz for α-helix, 3_{10}-helix, and β-sheet, respectively. The observed $^3J_{HN\alpha}$ coupling constants of **Y0**−**Y6** are listed in Table 3. The $FH^{NMR}_{^3J_{HN\alpha}}$ of the peptides calculated from the $^3J_{HN\alpha}$ coupling constants are listed in Table 1. These data suggest that **Y3** and **Y4** are as helical as **Y0**, whereas **Y5** and **Y6** are not half as helical as **Y0**.

The temperature dependence of δ_{HN} was used to characterize the involvement of the backbone amide in intramolecular hydrogen bonding.[33] For small peptides, temperature coefficients along the peptide sequence can be correlated with different types of secondary structure.[34] Temperature coefficients of hydrogens of backbone amides in **Y0**−**Y6** (Table 4) suggest that backbone amides of the first four residues are not involved in intramolecular hydrogen bonding, whereas the rest of the backbone amides are. The hydrogen bonding pattern inferred by the amide temperature coefficients are consistent with the hydrogen bonding pattern of the helical structure, because the amide of the N_{cap} residue and the first three backbone amides in the N-terminal part of a helix are not engaged in backbone intramolecular hydrogen bonds.

TABLE 3: $^3J_{HN-HC\alpha}$ Coupling Constants (Hz) from NMR Analyses of Y0−Y6[a]

residue	Y0	Y1	Y2	Y3	Y4	Y5	Y6
1	4.7	5.4	4.7	4.0	3.7	5.3	4.7
2	4.9	5.7	6.0	4.7	4.7	5.0	5.3
3	4.7	4.7	4.6	5.0	4.7	5.0	5.0
4	4.7	5.0	4.8	4.7	5.3	5.7	5.3
5	4.7	5.0	5.0		5.0	5.7	5.0
6	4.7	4.7			5.0	5.4	6.3
7	4.7	4.7		4.7	5.0	5.4	5.6
8	5.7	5.7	6.4	5.4	5.5	6.3	6.1
9	4.7	4.7	4.7		4.8	4.7	5.4
10	4.7	5.4	4.7	4.7	4.3	5.4	5.4
11	5.4	4.7	4.7	5.7	5.3	6.7	6.0
12	4.7	4.7	4.7		5.3	5.7	5.7
av	4.9	5.0	5.1	4.9	4.9	5.5	5.5

[a] The uncertainty is ±0.3 Hz.

TABLE 4: Temperature Coefficients (ppb/K) of Backbone Amide Hydrogens in Y0−Y6

residue	Y0	Y1	Y2	Y3	Y4	Y5	Y6
1	−13.0	−10.4	−13.0	−12.8	−13.9	−12.4	−12.7
2	−13.0	−8.2	−15.0	−12.4	−15.2	−12.0	−12.9
3	−10.2	−12.0	−7.0	−11.0	−10.9	−10.2	−10.3
4	−7.0	−8.2	−9.0	−3.8	−10.0		−5.6
5	−5.2 to −3.8	−4.4	−3.0		−5.5		−4.9
6	−5.2 to −3.8				−4.0	−6.8	−7.1
7	−5.2 to −3.8			−3.4	−4.0	−2.8	−6.6
8	−1.6	−1.4	−3.0	−5.0	−5.5	−1.6	−4.4
9	−1.6	−3.8			−2.0	−5.2	−4.9
10	−0.4	−0.6	−2.0		1.5	−4.8	−4.9
11	4.8	2.8	1.0	1.0	5.6	−0.6	−4.4
12	4.7	−0.6			2.5	−3.6	−2.9

The slight dispersion of the αCH and βCH resonances resulted in extensive overlap of the αCH−NH and the αCH−βCH regions, even in the 2D correlation spectra. Thus, most of αCH−NH(*i*,*j*) and αCH−βCH(*i*,*j*) NOEs were not individually observable. Only few sequential αN(*i*,*i*+1) NOE connectivities were observed, whereas most of the NN(*i*,*i*+1) and NN(*i*,*i*+2) connectivities were found in resolved areas (data not shown).

Figure 1 summarizes the observed NOE correlations between the aromatic ring of Tyr and the backbone amide protons in **Y1**−**Y6**. NOE cross-peaks between protons of the aromatic ring and the (*i*) and (*i*+1) amide protons were found in all peptides. Most NOE cross-peaks were observed in **Y5** (Figure 2), possibly because the **Y5** sample prepared for NMR had the highest concentration of all the peptides investigated (see methods). As a result, the NOESY spectrum of **Y5** had the best signal-to-noise ratio. NOE cross-peaks between αCH and βCH and aromatic ring protons were also observed, but these were not individually assignable.

Molecular Dynamics Calculation. The evolution of the structural properties of **Y5** during the simulation is shown in Figure 3. The α-helical structure was present in **Y5** throughout the trajectory except between 10 000 and 11 000 ps. The

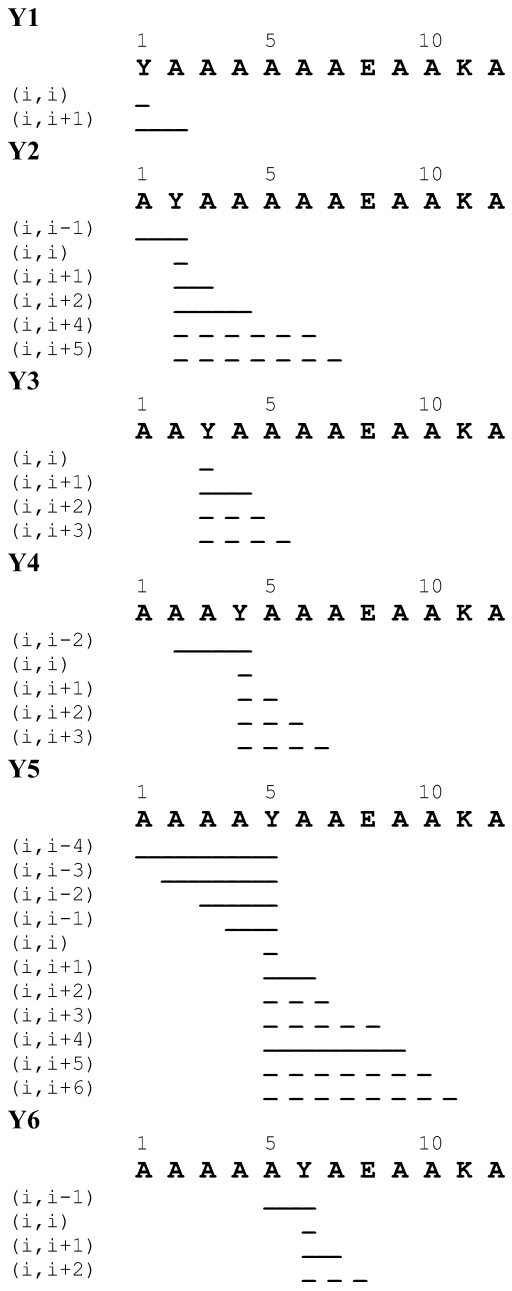

Figure 1. NOE cross-peaks between hydrogens of the aromatic ring of Tyr and the backbone amide protons in **Y1**−**Y6**. Solid bars indicate the observed NOEs. Dashed lines indicate NOEs whose existence or absence cannot be confirmed due to overlap with intraresidue cross-peaks.

orientation of the Tyr5 side chain was 66.52% *t*, 33.45% *g*−, and 0.03% *g*+. The effect of the aromatic ring on the δ_{HN} and $\delta_{\alpha CH}$ is represented in Figure 3C. The proximity of the aromatic ring to the HN and αCH protons causes the value of δ_{ring}^{HN} and $\delta_{ring}^{\alpha CH}$ to be other than zero. Values of less than −0.5 ppm δ_{ring}^{HN} and $\delta_{ring}^{\alpha CH}$, respectively, are indicative of Ar−HN[50−52] and of π−CH interactions.[53] In *t* orientation of the Tyr5 side chain, Ar(*i*)−HN(*i*+4) and π(*i*)−CH(*i*+1 and *i*+4) interactions were in the selected α-helical structures of **Y5**. Furthermore, when the Tyr5 side chain was in the *g*− orientation, Ar(*i*)−HN(*i* and *i*−4) and π(*i*)−CH(*i*, *i*−3, and *i*+4) interactions existed. Similar relationships were observed between δ_{ring}^{HN} and $\delta_{ring}^{\alpha CH}$ values and the α-helical structure of the other peptides investigated.

Average δ_{HN} and $\delta_{\alpha CH}$ values along a trajectory are provided in the Supporting Information. In the selected α-helical structures of the peptides, when the Tyr side chain was in *t* orientation, the aromatic ring caused positive ring shifts for the HN of *i*, *i*+1 and for the αCH of *i*, *i*+3, *i*+4 and negative ring shifts for the HN of *i*+3, *i*+4, *i*+5 and for the αCH of *i*+3, *i*+4. In *g*− orientation, the aromatic ring caused positive ring shifts for the HN of *i*+1 and for the αCH of *i*, *i*−3 and negative ring shifts for the HN of *i*, *i*−1, *i*−4 and for the αCH of *i*−1, *i*−4. The effect of the aromatic ring on δ weakened throughout the trajectory due to non-α-helical structures and to the structural dynamics of the aromatic side chain. Thus, only selected residues had detectable ring shifts which could be correlated with the α-helical structure of the peptides. For **Y1**−**Y6** the average δ_{ring}^{HN} was 0.08 ppm for the residue in position *i*, 0.06 ppm in *i*+1, −0.07 ppm in *i*+3, and −0.13 ppm in *i*+4. Furthermore, the average $\delta_{ring}^{\alpha CH}$ was 0.10 ppm for the residue in position *i*, −0.03 ppm in *i*+1, −0.04 ppm in *i*+3, and −0.07 in *i*+4.

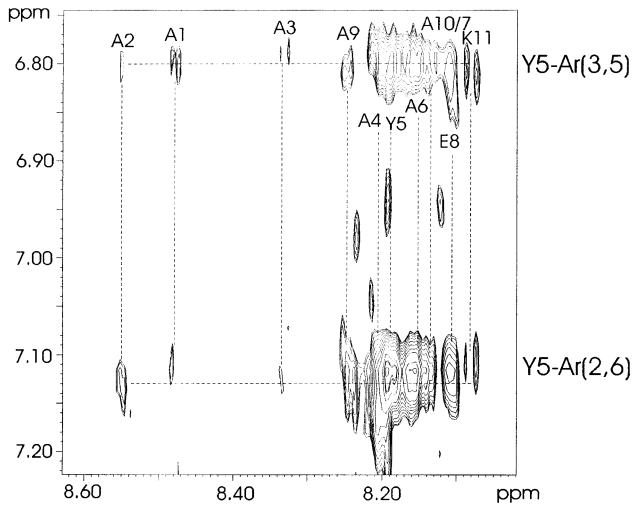

Figure 2. Contour plot showing the region of the NOESY spectrum with NOE cross-peaks between hydrogens of the aromatic ring of Tyr[5] and the backbone amide protons of **Y5**.

Table 5 summarizes the distribution of torsion angle χ^1 of Tyr in the selected α-helical structures of **Y1**−**Y6** and of Tyr, Phe, and Trp in different positions in α-helices of proteins. The distribution of χ^1 of Tyr in selected α-helical structures of **Y1**, **Y3**, and **Y4** differed from that of Tyr, Phe, and Trp in the N-terminal positions. Conversely, the distribution of χ^1 of Tyr was similar in selected α-helical structures of **Y5** and **Y6** to the distribution of χ^1 of Tyr, Phe, and Trp in inner positions of protein helices. The difference in distribution of χ^1 in **Y2** and **Y1**, **Y3**, and **Y4** could be due to the proximity of the Tyr side chain in the *g*− orientation to the carbonyl function of the acetyl group, thereby causing frequent aromatic-carbonyl (Ar−CO) interactions. Such interaction could be partially responsible for the high percentage of *g*− orientation of the Tyr side chain in **Y2**.

The Tyr side chain in the selected α-helical structures of **Y1**−**Y6** limited solvent access to the backbone atoms. The extent of solvent access depended on the orientation of the Tyr side chain and on the position of the Tyr in the peptides. Table 6 lists the solvent accessible surface areas (SASAs) of selected backbone atoms. With the *t* orientation of the Tyr side chain, the SASAs of backbone carbonyl and amide groups in position *i* and *i*+4 were approximately 80% lower than with the *g*− orientation. With the *g*− orientation of the Tyr side chain in **Y4**−**Y6,** the SASAs of backbone carbonyl and backbone amide groups in position *i*−4 and *i*, respectively, were about 90% lower than with the *t* orientation. The Tyr side chain in *g*− orientation decreased SASAs of NH(*i*) and CO (*i*−4) approximately 3 times

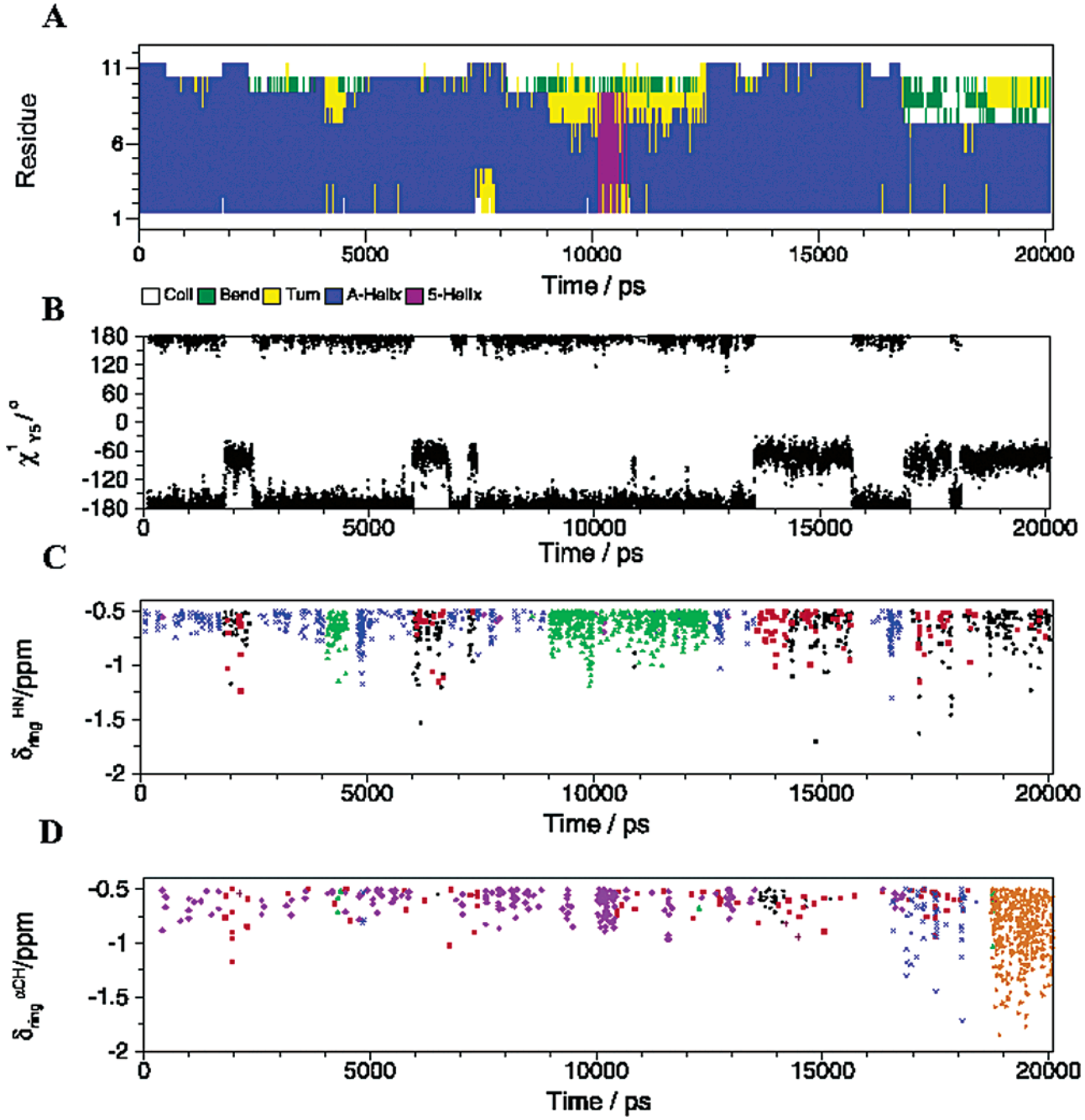

Figure 3. Evolution of the structural properties of **Y5** during the trajectory: (A) secondary structure; (B) χ^1 torsion angle of Tyr^5; (C) δ_{ring}^{HN} of residue in positions $i-4$, black; i, red; $i+1$, magenta; $i+4$, blue; $i+5$, green; (D) $\delta_{ring}^{\alpha CH}$ of residue in positions $i-4$, black, $i-3$, orange; i, red; $i+1$, magenta; $i+4$, blue; $i+5$, green. (δ_{ring}^{HN} and $\delta_{ring}^{\alpha CH}$ values less than −0.5 ppm only are shown.)

more than it decreased the SASAs of CO(i) and NH($i+4$) in the t orientation. Large differences were observed between the SASAs of HN(i) of **Y1**−**Y3** and **Y4**−**Y6**.

The interaction energy of the hydroxyphenyl group of Tyr with the α-helical polypeptide backbone was calculated (Table 6). Interaction energies between the backbone and the hydroxyphenyl group of Tyr in t orientation in selected α-helical structures of **Y1**−**Y6** were similar. Interaction energies between the backbone and the hydroxyphenyl group of Tyr in the $g-$ orientation were similar in selected α-helical structures of **Y4**−**Y6** but lower in selected α-helical structures of **Y1**−**Y3**. Interaction energies between the aromatic ring of Tyr and the backbone were most negative in inner positions of α-helical peptide fragments of proteins. Interaction energies between the hydroxyphenyl group of Tyr and the backbone, in inner positions of α-helical polypeptide fragments of proteins, were approximately 6 and 10 kJ mol^{-1} lower in t and $g-$ orientations, respectively, than in selected α-helical structures of **Y5** and **Y6**. This energy difference was approximately halved when the α-helical polypeptide fragments from proteins were energy minimized. The minimization resulted primarily in weaker repulsion between the aromatic ring and the backbone carbonyl group of the aromatic residue, because the positive Lennard-Jones energy between these interacting groups decreased. Energy minimization of protein fragments, however, can lead to artifacts, because it overlooks the possible effects of the side chains from neighboring chains in the protein.

Figure 4 shows the energy map of aromatic−backbone interactions of Tyr in inner α-helices of proteins and in **Y6**. Differences between the two maps are the locations of local

TABLE 5: Percentage and Average (in Brackets) of the χ^1 Torsion Angle for Tyr in Selected α-Helical Structures of Y1−Y6 from Each Trajectory and for Tyr, Phe, and Trp in Different Positions of α-Helical Peptide Fragments from Proteins

polypeptide	g−	*t*	g+
Y1	9.32 (−75.90 ± 19.09)	90.68 (−170.19 ± 13.76)	
N_{cap}−Y	74.51 (−63.90 ± 14.15)	16.17 (−176.66 ± 16.31)	9.31 (58.94 ± 10.01)
N_{cap}−F	65.99 (−63.90 ± 14.15)	8.12 (−176.15 ± 16.46)	8.12 (62.22 ± 23.17)
N_{cap}−W	65.59 (−67.62 ± 10.41)	19.35 (−165.88 ± 16.76)	15.05 (59.49 ± 9.17)
Y2	54.66 (−65.67 ± 14.63)	45.11 (170.33 ± 14.56)	0.23 (66.03 ± 5.37)
N1−Y	34.49 (−72.06 ± 13.79)	50.00 (−177.34 ± 11.17)	15.50 (70.17 ± 20.01)
N1−F	28.57 (−68.52 ± 13.99)	65.17 (−176.22 ± 10.28)	5.71 (74.06 ± 12.99)
N1−W	45.08 (−68.83 ± 15.99)	34.83 (−175.77 ± 12.37)	19.35 (67.00 ± 7.32)
Y3	0.18 (−116.12 ± 3.78)	99.82 (−173.98 ± 13.58)	
N2−Y	32.09 (−66.61 ± 8.97)	54.88 (179.89 ± 11.49)	13.02 (67.68 ± 11.97)
N2−F	31.80 (−67.40 ± 14.14)	63.59 (−177.74 ± 12.53)	4.61 (70.76 ± 12.98)
N2−W	27.43 (−66.61 ± 16.56)	35.40 (−175.40 ± 9.23)	37.17 (65.01 ± 13.74)
Y4	8.26 (−84.32 ± 16.33)	91.68 (−175.40 ± 16.26)	0.07 (110.51 ± 9.04)
N3−Y	38.75 (−66.02 ± 11.13)	60.42 (179.66 ± 9.73)	0.83 (49.23 ± 2.36)
N3−F	34.57 (−65.79 ± 11.19)	64.61 (179.92 ± 10.77)	0.82 (73.75 ± 12.09)
N3−W	43.69 (−70.11 ± 14.59)	55.34 (−178.56 ± 10.61)	0.97 (77.34 ± 0.00)
Y5	40.28 (−70.96 ± 14.99)	59.67 (−175.01 ± 15.05)	0.05 (111.01 ± 4.72)
Y6	44.71 (−70.52 ± 14.98)	55.29 (−172.81 ± 15.67)	0.00
N4−C4−Y	38.40 (−74.03 ± 11.67)	60.10 (179.51 ± 11.85)	1.50 (73.30 ± 9.58)
N4−C4−F	37.22 (−75.80 ± 11.44)	62.03 (178.90 ± 13.99)	0.75 (70.31 ± 12.62)
N4−C4−W	32.40 (−75.28 ± 13.96)	65.36 (−178.03 ± 11.63)	2.23 (86.44 ± 18.73)
C3−Y	42.70 (−75.36 ± 13.40)	56.18 (179.45 ± 10.85)	1.12 (74.42 ± 13.67)
C3−F	58.62 (−74.17 ± 11.60)	41.07 (178.93 ± 13.05)	0.31 (77.12 ± 0.00)
C3−W	43.85 (−70.18 ± 13.15)	53.08 (−179.85 ± 16.16)	3.08 (76.35 ± 7.18)
C2−Y	46.81 (−71.62 ± 11.47)	50.64 (179.60 ± 12.20)	2.55 (85.68 ± 14.39)
C2−F	56.12 (−71.78 ± 11.02)	41.73 (178.55 ± 11.68)	2.16 (65.87 ± 13.12)
C2−W	43.48 (−67.79 ± 8.99)	53.26 (179.12 ± 10.58)	3.26 (77.46 ± 5.71)
C1−Y	79.69 (−63.53 ± 12.11)	16.97 (−177.30 ± 15.44)	3.34 (58.35 ± 11.52)
C1−F	82.49 (−64.83 ± 12.12)	16.50 (−179.77 ± 10.33)	1.01 (50.48 ± 30.39)
C1−W	65.22 (−68.65 ± 11.46)	33.33 (−174.64 ± 13.47)	1.45 (56.31 ± 0.00)
C_{cap}−Y	80.71 (−63.72 ± 11.79)	15.99 (−179.22 ± 12.47)	3.30 (56.05 ± 20.27)
C_{cap}−F	85.58 (−65.53 ± 12.80)	11.35 (−171.96 ± 15.08)	3.07 (61.08 ± 23.42)
C_{cap}−W	66.67 (−67.22 ± 10.80)	25.00 (−175.79 ± 10.73)	8.33 (62.70 ± 12.45)

TABLE 6: Solvent Accessible Surface Area (SASA) (Å^2) of Selected Backbone Amide (HN), Backbone Carbonyl (CO), and Hydroxyphenyl Groups in the Selected α-Helical Structures of Y1−Y6 with Different Orientations of the Tyr Side Chain

	(*i*)N	(*i*)H	(*i*−4)C[a]	(*i*−4)O[a]	$\Sigma_{NH..CO}$	(*i*)C	(*i*)O	(*i*+4)N	(*i*+4)H	$\Sigma_{CO..NH}$	(*i*)hydroxyphenyl
Y1											
g−	1.84	4.01	3.76	3.72	13.32	1.64	2.94	0.90	0.05	5.53	177.48
t	3.81	7.70	4.66	9.47	25.64	0.16	0.46	0.50	0.01	1.12	147.26
Y2											
g−	1.10	3.38	5.61	16.84	26.93	1.64	2.60	0.91	0.02	5.17	164.38
t	2.06	5.70	5.43	15.39	28.58	0.06	0.64	0.73	0.02	1.45	157.69
Y3											
g−											
t	1.63	2.29	3.97	2.41	10.30	0.02	0.73	0.84	0.01	1.61	158.86
Y4											
g−	0.20	0.04	1.58	1.26	3.09	0.76	0.79	0.33	0.00	1.88	150.39
t	1.47	1.08	5.19	17.63	25.37	0.01	0.20	0.19	0.00	0.40	134.83
Y5											
g−	0.11	0.00	0.09	0.06	0.27	1.56	3.04	0.82	0.02	5.44	123.13
t	0.74	0.03	0.93	1.42	3.11	0.03	0.55	0.71	0.01	1.31	147.68
Y6											
g−	0.10	0.00	0.21	0.14	0.45	1.52	3.25	0.79	0.02	5.60	143.75
t	1.11	0.03	1.83	3.51	6.48	0.03	0.58	0.65	0.01	1.27	157.49

[a] Due to the absence of the (*i*−4)CO group in **Y1**−**Y3**, the CO of the acetyl group was used for the SASA calculations. The values for **Y**3 with the Tyr side chain in g− orientation are statistically insignificant.

minima and maxima. The low energies (green regions) of the *t* and *g*− orientations of the Tyr side chain of the two maps are similar. Thus, the frequent transition of the Tyr side chain between *t* and *g*− during simulations of the model peptides could be facilitated by the lack of energy barriers between these two conformations.

Table 8 lists interaction energies between the hydroxyphenyl group of Tyr and backbone groups in selected α-helical structures of **Y5** and in α-helical protein fragments. Interaction energies in **Y5** were similar to those in protein fragments, with one exception. Interaction energies between the aromatic ring and CO(*i*) were 3.36 kJ mol^{-1} more positive in α-helical proteins fragments than in the investigated model peptides.

An *i*−3/*i*+3 interaction was observed between the side chains of Glu^8 and Lys^{11} as they formed a salt bridge in 17.00, 11.11, 14.13, 23.17, 34.54, 15.45, and 6.15%, respectively, of the selected α-helical structures of **Y0**−**Y6**. Furthermore, the hydroxyl group of the aromatic side chain of the Tyr^4 formed a hydrogen bond with the side chain carboxyl group of Glu^8 in 34.54% of the selected α-helical structures of **Y4**.

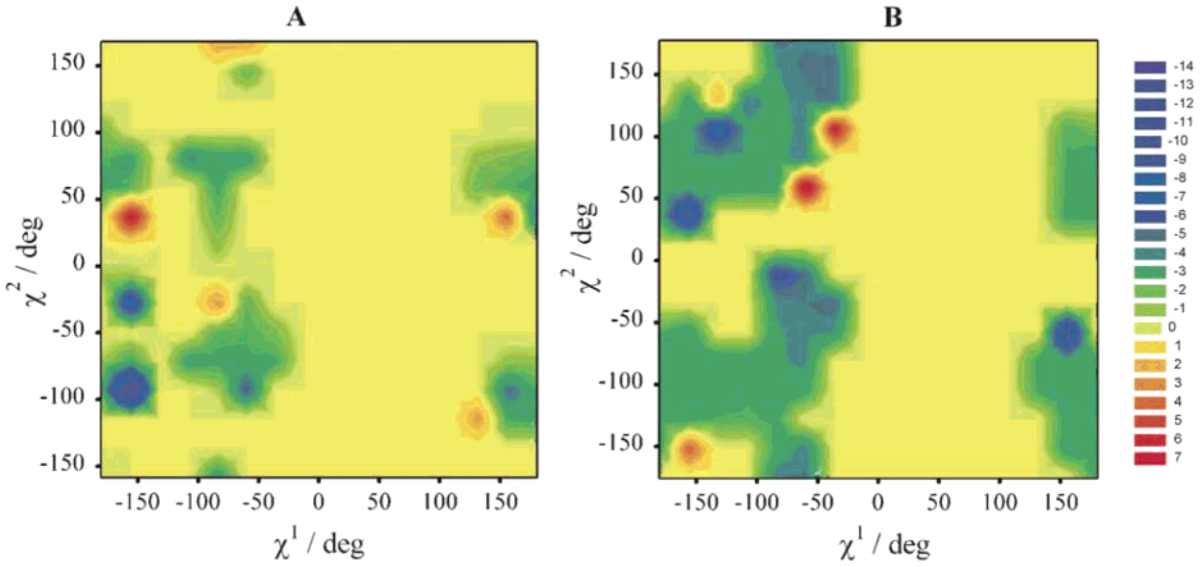

Figure 4. Interaction energy (kJ mol^{-1}), between the hydroxyphenyl group of Tyr, in inner positions of the α-helix, and the backbone in (A) α-helical polypeptide fragments from proteins and in (B) selected α-helical structures of **Y6** by varying χ^1 and χ^2 of Tyr.

TABLE 7: Interaction Energy (kcal mol^{-1}) between the Side Chain Aromatic Ring and Backbone in Selected α-Helical Structures of Y1−Y6 and in Inner Positions of α-Helical Protein Fragments

	t	*g*−	av
Y1	−3.90 ± 1.23	−2.30 ± 0.56	−3.74 ± 1.28
Y2	−3.36 ± 0.85	−3.07 ± 0.86	−3.20 ± 0.87
Y3	−3.20 ± 0.43	−3.50 ± 0.29	−3.20 ± 0.43
Y4	−3.53 ± 0.52	−3.61 ± 0.49	−3.54 ± 0.54
Y5	−3.97 ± 0.77	−4.97 ± 1.20	−4.38 ± 1.09
Y6	−3.44 ± 0.42	−4.15 ± 0.63	−3.75 ± 0.68
Tyr	−2.25 ± 1.12	−2.06 ± 1.83	−2.18 ± 1.33
Phe	−3.18 ± 1.29	−2.86 ± 1.91	−3.06 ± 1.56
Trp	−6.43 ± 1.22	−5.78 ± 1.02	−6.21 ± 1.19

Discussion

Aromatic−Backbone Interactions. The energy of interaction between the aromatic ring of Tyr and the α-helical polypeptide backbone has a complex dependence on side chain rotamer orientations and the dynamics of the α-helical backbone. Depending on torsion angles χ^1 and χ^2 of the aromatic residue, the interaction energy of the aromatic ring and the α-helical backbone is dominated by the Ar−HN interaction, the π−CH interaction, and the Ar−CO interaction (Figure 5). Accurate determination of interaction energies of these complexes requires high-level ab initio studies; therefore, interaction energies calculated with the GROMACS force field[38] may yield only estimates of the strength of the aromatic−backbone interactions. Furthermore, the GROMACS force field can only approximate the strength of possible interaction between the macrodipole of the helix and the quadrupole of the aromatic ring.

The large difference between interaction energies in selected α-helical structures of **Y5** and **Y6** and in inner positions of α-helical fragments of proteins may originate from the interactions of the aromatic side chain either with other side chains in the α-helix or with nearby side chains in the protein. Such side chain−side chain interactions may force the aromatic ring into conformations in which its interaction with the backbone is not energetically as favorable as in an Ala-based α-helix. This is supported by the differences in average χ^1 torsion angle values of the *t* and *g*− orientations.

NOE cross-peaks between hydrogens of the aromatic ring of Tyr and backbone amide hydrogens could be indicative of the proximity and orientation of the aromatic ring to the backbone. The distances between the hydrogens of the aromatic ring and hydrogen of backbone amides vary with the orientation of the aromatic side chain in the α-helix. In the *t* orientation, only limited rotational states ensure short enough distances between the ring hydrogens and the *i*+4 amide hydrogen to result in NOE cross-peaks. This is also true in the *g*− orientation for distances between the aromatic ring hydrogens and backbone *i*−3 and *i*−4 amide hydrogens. Therefore, these NOEs may not be observable. NOEs, however, between 2,6 hydrogens of the aromatic ring and *i*, *i*+1 amide hydrogens in both *t* and *g*− orientations are detectable. This is in agreement with the observed NOEs (Figure 3). Therefore, all other NOEs must have originated from non-α-helical structures.

Solvent Screening of the Backbone. Side chain interference with solvation of peptide backbone groups is a major determinant of helical propensities.[54−56] The shielding of the backbone from water by the aromatic side chain in helices desolvates some polar backbone groups. The decrease in the SASA of backbone polar groups lowers the electrostatic solvation free energy of these groups and affects the helix stability.[54] Nevertheless, the decline in the number of solvent water molecules around the C═O and H−N groups, due to the shielding effect of the aromatic side chain, forces these polar groups to interact less with the solvent and more with each other.[56,57]

Rotamer Preferences of the Side Chains of Aromatic Residues in α-Helices. The difference in the distribution of χ^1 for Tyr in α-helical structures of **Y1**, **Y3**, and **Y4** selected from the trajectories and of χ^1 of Tyr, Phe, and Trp in the N-terminal positions of α-helical proteins fragments suggests that residues preceding the N_{cap} influence the rotational freedom of the aromatic side chain. Therefore, studies of model peptides intended to elucidate the helical propensities of amino acid residues may produce accurate results only when residues precede the N_{cap}. The agreement of the χ^1 distribution in selected α-helical structures of **Y5** and **Y6** with that for the aromatic residues in inner positions of α-helices in proteins suggests that interactions either with other side chains in the helix or with nearby chains in the protein do not influence this distribution. Interactions of the aromatic ring with other side chains, however, should be responsible for the difference in the average values of χ^1 in *t* and *g*− orientation.

TABLE 8: Interaction Energy (kcal mol^{-1}) between the Hydroxyphenyl Group of Tyr and Backbone Groups in Selected α-Helical Structures of Y5 and Inner Positions of α-Helical Peptide Fragments from Proteins[a]

	(*i*)H−N			(*i*−4)O=C		(*i*+4)H−N		(*i*)O=C			(*i*+1)H−N		(*i*−3)O=C		
polypeptide	E_C	E_{LJ}	E_{LJ14}	E_C	E_{LJ}	E_C	E_{LJ}	E_C	E_{LJ}	E_{LJ14}	E_C	E_{LJ}	E_C	E_{LJ}	ΣE
t															
Y5	0.05	−0.23	−0.14	0.03	−0.20	−0.10	−0.11	0.11	−0.93	0.51	0.13	−0.48	−0.15	−0.33	−1.79 ± 0.31
Tyr	0.06	−0.23	−0.13	0.04	−0.17	−0.05	−0.11	0.27	−0.67	0.90	0.13	−0.47	−0.12	−0.29	−0.83 ± 0.85
g−															
Y5	−0.20	−0.45	0.04	0.28	−1.05	0.00	−0.02	−0.24	−0.40	−0.10	−0.03	−0.16	0.04	−0.36	−2.10 ± 1.23
Tyr	0.05	−0.27	0.14	0.13	−0.88	0.00	−0.02	−0.15	−0.43	−0.10	0.00	−0.15	0.06	−0.32	−2.54 ± 0.76

[a] E_C is the electrostatic interaction energy calculated with the Coulomb relationship. E_{LJ} and E_{LJ14} are the van der Waals interaction energies calculated with the Lennard-Jones relationship.

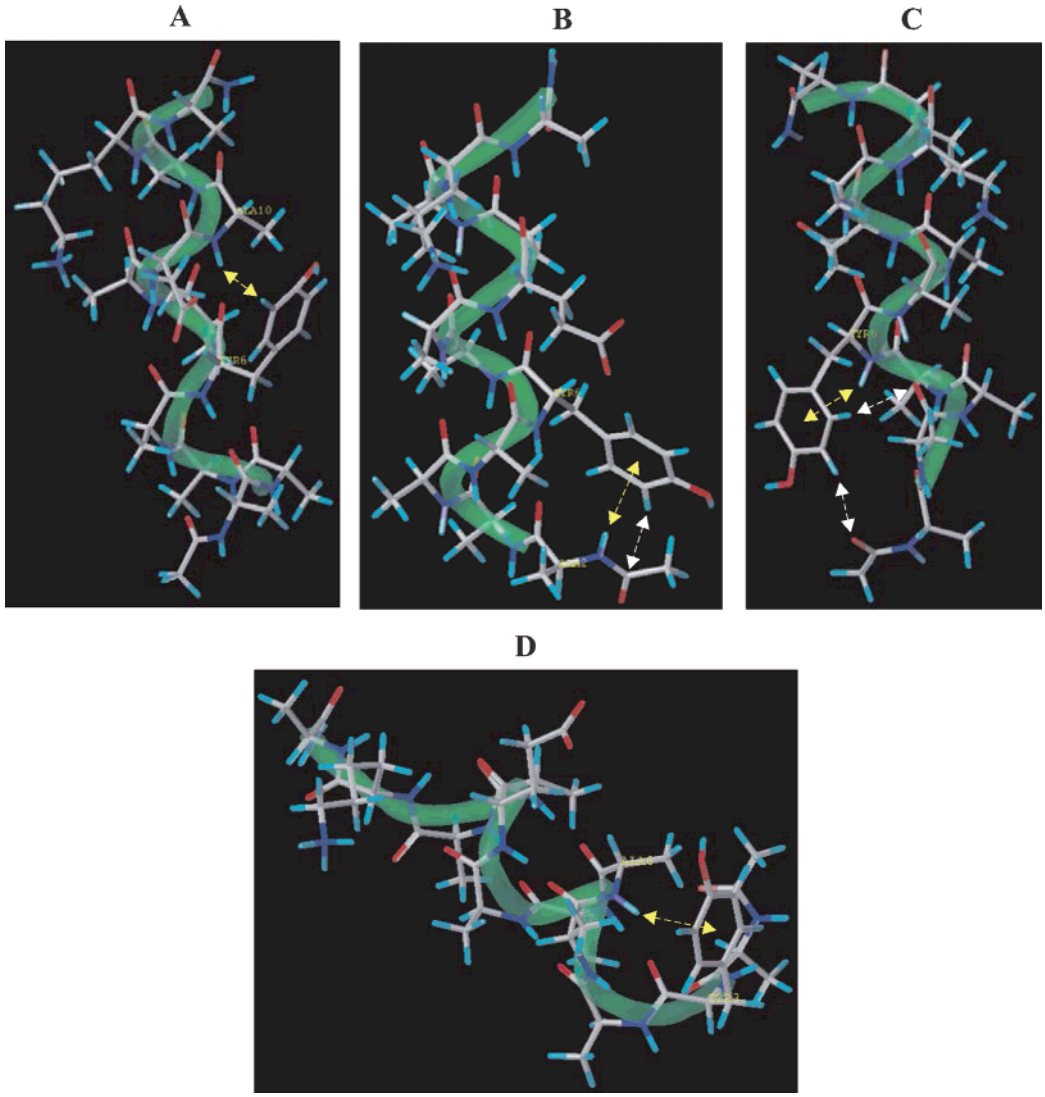

Figure 5. Snapshots from the trajectories. Ar−HN and (aromatic)C−H···O=C interactions are indicated by yellow and white arrows, respectively. Green tubes indicate α-helices. (A) Ar(*i*)−HN(*i*+4) interaction between the aromatic ring of Tyr^5 and the backbone amide of Ala^9 in **Y5**. (B) Ar(*i*)−HN(*i*−4) interaction between the aromatic ring of Tyr^5 and the backbone amide of Ala^1 and (aromatic)C−H···O=C interaction between the C−H of the aromatic ring of Tyr^5 and the carbonyl of the acetyl group in **Y5**. (C) Ar(*i*)−HN(*i*) interaction between the aromatic ring of Tyr^5 and the backbone amide of Tyr^5 and two (aromatic)C−H···O=C interactions between C−H of the aromatic ring of Tyr^5 and the carbonyl of Ala^2 and of the acetyl group in **Y5**. (D) Ar(*i*)−HN(*i*+3) interaction between the aromatic ring of Tyr^2 and the backbone amide of Ala^5 in **Y2**.

All the phase space is available to the aromatic side chain when in the (*t*) orientation, whereas in the *g*− orientation, χ^1 can be only between −120° and −40° approximately. The *g*+ orientation of an aromatic side chain is not possible in an ideal α-helix.[58] Several cases were found in the PDB, however, where the side chain of the aromatic residue was in *g*+ orientation. These residues are located in parts of α-helices, which are forced to deviate from the average α-helical structure, for example, when Pro precedes the aromatic residue in either position *i*−1, *i*−2, or *i*−3 to cause a kink in the helix.

Helix Content of the Peptides. The helical content of a peptide can be determined using $\delta_{\alpha CH}$ values.[59,35] The effect of the aromatic ring on $\delta_{\alpha CH}$ values in different secondary structures, however, is not clear. Because $\delta_{\alpha CH}$ is dependent on the secondary structure of a polypeptide chain as well as on the position of the aromatic residue therein,[60] changes in $\delta_{\alpha CH}$

can result from the proximity of the aromatic ring to the αCH and/or from the modified degree of helical structure of the polypeptide. The average $\delta_{ring}^{\alpha CH}$, derived from the MD simulations, characteristic of helix, was not significant because the observed negative δ_{ring} cancels the positive δ_{ring}. Non-α-helical conformations, however, can cause such $\delta_{ring}^{\alpha CH}$ values that result in large errors in $FH_{\delta_{\alpha CH}}^{NMR}$ calculations. For example, in the MD trajectory of **Y1**, the sum of all $\delta_{ring}^{\alpha CH}$ was −0.32, whereas in the MD trajectory of **Y2**, the sum of all $\delta_{ring}^{\alpha CH}$ was 0.04. This can result in errors up to 15%.

$FH_{^3J_{HN\alpha}}^{NMR}$ values revealed that Tyr destabilized the helical structure in **Y5** and **Y6** compared with **Y0**, whereas the effect of Tyr on the stability of the helix is similar to that of the Ala in **Y0**−**Y4**. $FH_{^3J_{HN\alpha}}^{NMR}$ values should be regarded with care, because the errors associated with the determination of $^3J_{HN\alpha}$ and $FH_{^3J_{HN\alpha}}^{NMR}$ are up to ±0.3 Hz and ±13%, respectively. Because the aromatic ring currents have a direct effect on the $\delta_{\alpha CH}$ values, the $FH_{^3J_{HN\alpha}}^{NMR}$ values are considered to be more accurate than the $FH_{\delta_{\alpha CH}}^{NMR}$ values.

The first three backbone amide groups in the N-terminal part of a helix are not involved in a hydrogen bond with a backbone carbonyl group, whereas those in the inner helix are. Therefore, the lower helicity of **Y5** and **Y6** than of **Y1**−**Y4**, indicated by $FH_{^3J_{HN\alpha}}^{NMR}$, can be attributed to a different extent of solvation of the backbone amide group of Tyr in the N-terminal than in the inner part of the helix. In the peptides investigated, the shielding from the solvent of the Tyr backbone amide group by the Tyr side chain in *g*− orientation resulted in different degrees of solvation in the N-terminal and inner helical positions. The position of Tyr in the helical structure could also affect the stability of the helix. In **Y1**−**Y3**, when Tyr is in the N-terminal part of the helix, possible interaction between the quadrupole of the aromatic ring and the helix macrodipole would favor helix stability. Conversely, when the Tyr side chain is in *t* orientation facing the C-terminus in **Y5** and **Y6**, the interaction between the aromatic ring and the macrodipole of the helix would be unfavorable to helix stability. The observed hydrogen bond between the hydroxyl group of the aromatic side chain of Tyr^4 and the side chain carboxyl group of Glu^8 in **Y4** may contribute to the stability of the helical structure.

Conclusion

The investigation of the interaction between the aromatic ring of an amino acid and the α-helical polypeptide backbone in model peptides and proteins revealed a complex network of weakly polar interactions. The present investigation shows that aromatic−backbone interaction is a common phenomenon in proteins. The origin of the aromatic−backbone interaction in α-helices was the result of the Ar−HN, π−HC, and Ar−CO interactions. These interactions are weak separately but, in combination, they can have strong influence on the stability of polypeptide structure. The presence of the aromatic−backbone interactions dramatically decreased the solvation of some amide and carbonyl groups in the helical backbone due to the shielding effect of the aromatic ring from the solvent. These factors, in delicate balance, determine the influence of the aromatic side chain on the stabiltiy of helical structure.

Acknowledgment. This work was supported by grants from the NSF (EPS-9720643), the BRIN program of the National Center for Research Resources (NIH Grant Number 1 P20RR16469), the Carpenter Endowed Chair in Biochemistry, Creighton University, and grants from the Hungarian National Research Foundation (OTKA T 042567, T 034515). Thanks to Attila Borics for critical reading of the manuscript.

Supporting Information Available: Tables of NMR data, ring shifts, and number of α-helical sstructures. This material is available free of charge via the Internet at http://pubs.acs.org.

References and Notes

(1) Burley, S. K.; Petsko, G. A. *Adv. Protein Chem.* **1988**, *39*, 125−189.
(2) (a) Hobza, P.; Havlas, Z. *Chem. Rev.* **2000**, *100*, 4253−4264. (b) Meyer, E. A.; Castellano, R. K.; Diederich, F. *Angew. Chem.* **2003**, *42*, 1210−1250.
(3) Dougherty, D. A. *Science* **1996**, *271*, 163−168.
(4) Tsuzuki, S.; Honda, K.; Uchimaru, T.; Mikami, M.; Tanabe, K. *J. Am. Chem. Soc.* **2000**, *122*, 3746−3753.
(5) Tsuzuki, S.; Honda, K.; Uchimaru, T.; Mikami, M.; Tanabe, K. *J. Am. Chem. Soc.* **2000**, *122*, 11450−11458.
(6) Worth, G. A.; Wade, R. C. *J. Phys. Chem.* **1995**, *99*, 17473−17482.
(7) Duan, G.; Smith, V. H., Jr.; Weaver, D. F. *Chem. Phys. Lett.* **1999**, *310*, 323−332.
(8) (a) Tóth, G.; Watts, C. R.; Lovas, S.; Murphy, R. F. *Proteins: Struct. Funct. Genet.* **2001**, *43*, 373−381. (b) Borics, A.; Murphy, R. F.; Lovas, S. *Biopolym.: (Biospectrosc.)* **2003**, *72*, 21−24.
(9) Burley, S. K.; Petsko, G. A. *Science* **1985**, *229*, 23−28.
(10) Chipot, C.; Jaffe, R.; Maigret, B.; Pearlman, D. A.; Kollman, P. A. *J. Am. Chem. Soc.* **1996**, *118*, 11217−11224.
(11) Muller-Dethlef, K.; Hobza, P. *Chem. Rev.* **2000**, *100*, 143−167.
(12) Galivan, J. P.; Dougherty, D. *Proc. Natl. Acad. Sci. U.S.A.* **1999**, *96*, 9459−9464.
(13) Andrew, C. D.; Bhattacharjee, S.; Kokkoni, N.; Hirst, J. D.; Jones, G. R.; Doig, A. J. *J. Am. Chem. Soc.* **2002**, *124*, 12706−12714.
(14) Tsou, L. K.; Tatko, C. D.; Water, M. L. *J. Am. Chem. Soc.* **2002**, *124*, 14917−14921.
(15) Padmanabhan, S.; Baldwin, R. L. *J. Mol. Biol.* **1994**, *241*, 706−713.
(16) Muñoz, V.; Blanco, F. J.; Serrano, L. *Nature Struct. Biol.* **1995**, *2*, 380−385.
(17) Armstrong, K. M.; Fairman, R.; Baldwin, R. L. *J. Mol. Biol.* **1993**, *230*, 284−291.
(18) Fernandez-Recio, J.; Vazquez, A.; Civera, C.; Sevilla, P.; Sancho, J. *J. Mol. Biol.* **1997**, *267*, 184−197.
(19) Bhattacharyya, R.; Samanta, U.; Chakrabarti, P. *Protein Eng.* **2002**, *15*, 91−100.
(20) Vijayakumar, M.; Qian, H.; Zhou, H. *Proteins: Struct. Funct. Genet.* **1999**, *34*, 497−507.
(21) (a) Steiner, T.; Koellner, G. *J. Mol. Biol.* **2001**, *305*, 535−557. (b) Bhattacharjee, S.; Tóth, G.; Lovas, S.; Hirst, J. D. *J. Phys. Chem. B* **2003**, *107*, 8682−8688.
(22) Bernstein, F. C.; Koetzle, T. F.; Williams, G. J.; Meyer, E. E., Jr.; Brice, M. D.; Rodgers, J. R.; Kennard, O.; Shimanouchi, T.; Tasumi, M. *J. Mol. Biol.* **1977**, *12*, 535−542.
(23) Scholtz, J. M.; Qian, H.; Robbins, V. H.; Baldwin, R. L. *Biochemistry* **1993**, *32*, 9668−9676.
(24) Lockhart, D. J.; Kim, P. S. *Science* **1993**, *236*, 198−201.
(25) Bernatowicz, M. S.; Daniels, S. D.; Köster, H. *Tetrahedron Lett.* **1989**, *30*, 4645−4648.
(26) Bax, A.; Davis, D. G. *J. Magn. Reson.* **1985**, *65*, 355−360.
(27) Kövér, K. E.; Uhrin, D.; Hruby, V. J. *J. Magn. Reson.* **1998**, *130*, 162−168.
(28) Kumar, A.; Ernst, R. R.; Wuthrich, K. *Biochem. Biophys. Res. Commun.* **1980**, *95*, 1−6.
(29) Lippens, G.; Dhalluin, C.; Wieruszeski, J. M. *J. Biomol. NMR* **1995**, *5*, 327−331.
(30) Wüthrich, K. *NMR of Proteins and Nucleic Acids*; Wiley-Interscience: New York, 1986.
(31) Smith, L. J.; Bolin, K. A.; Schwalbe, H.; MacArthur, M. W.; Thornton, J. M.; Dobson, C. M. *J. Mol. Biol.* **1996**, *255*, 494−506.
(32) Wishart, D. S.; Bigam, C. G.; Holm, A.; Hodges, R. S.; Sykes, B. *J. Biomol. NMR* **1995**, *5*, 67−81.
(33) Evans, J. N. S. *In Biomolecular NMR Spectroscopy*; Oxford University Press: New York, 1995; p 153.
(34) Austin, E. R.; Maplestone, A. R.; Sefler, M. A.; Liu, K.; Hruzewicz, N. W.; Liu, W. C.; Cho, S. H.; Wemmer, E. D.; Bartlett, A. P. *J. Am. Chem. Soc.* **1997**, *119*, 6461−6472.
(35) Lacroix, E.; Viguera, A. R.; Serrano, L. *J. Mol. Biol.* **1998**, *284*, 173−91.
(36) Wishart, D. S.; Sykes, B. D.; Richards, F. M. *J. Mol. Biol.* **1991**, *222*, 211−333.
(37) Serrano, L. *J. Mol. Biol.* **1995**, *254*, 322−333.

(38) van der Spoel, D.; Berendsen, H. J. C.; van Buuren, A. R.; Apol, E.; Muelenhoff, P. J.; Sijbers, A. L. T. M.; van Drunen, R. Nijenborgh 4, 9747 AG Groningen, The Netherlands, 1995. Internet: http://rugmdO.chem.rug.nl/~gmx.

(39) *Sybyl Users Manual*; Tripos Inc.: St. Louis, MO, 1996.

(40) Hess, B.; Bekker, H.; Berendsen, H. J. C.; Fraaije, J. G. E. M. *J. Comput. Chem.* **1997**, *18*, 1463−1472.

(41) Kabsch, W.; Sander, C. *Biopolymers* **1983**, *22*, 2577−2637.

(42) Hubbard, S. J.; Thornton, J. M. Department of Biochemistry and Molecular Biology, University College, London, 1993.

(43) Worth, G. A.; Nardi, F.; Wade, R. C. *J. Phys. Chem.* **1998**, *102*, 6260−6272.

(44) Nardi, F.; Kemmink, J.; Sattler, M.; Wade, R. C. *J. Biomol. NMR* **2000**, *17*, 63−77.

(45) Toth, G.; Lovas, S.; Murphy, R. F. *Internet J. Chem.* **1998**, *2*, http://www.IJC.com/articles/199v2/5/.

(46) Shimohigash, Y.; Nose, T.; Yamauchi, Y.; Maeda, I. *Biopolymers* **1999**, *51*, 9−17.

(47) Williamson, P. W.; Asakura, T. *J. Magn. Reson. Ser. B* **1993**, *101*, 67−71.

(48) Chakrabarti, P.; Chakrabarti, S. *J. Mol. Biol.* **1998**, *284*, 867−873.

(49) Karplus, M. *J. Chem. Phys.* **1959**, *30*, 11−15.

(50) Kemmink, J.; van Mierlo, C. P. M.; Scheek, R. M.; Creighton, T. E. *J. Mol. Biol.* **1993**, *230*, 312−322.

(51) Kemmink, J.; Creighton, T. E. *J. Mol. Biol.* **1993**, *234*, 861−878.

(52) Kemmink, J.; Creighton, T. E. *J. Mol. Biol.* **1995**, *243*, 251−260.

(53) Nishio, M.; Umezawa, Y.; Hirota, M.; Takeuchi, Y. *Tetrahedron* **1995**, *51*, 8665−8701.

(54) Avbelj, F.; Luo, P.; Baldwin, R. L. *Proc. Natl. Acad. Sci. U.S.A.* **2000**, *97*, 10786−10791.

(55) Luo, P.; Baldwin, R. L. *Proc. Natl. Acad. Sci. U.S.A.* **1999**, *96*, 4930−4935.

(56) Vila, J. A.; Ripoll, D. R.; Scheraga, H. A. *Proc. Natl. Acad. Sci. U.S.A.* **1997**, *97*, 13075−10791.

(57) (a) Levy, Y.; Jortner, J.; Becker, O. M. *Proc. Natl. Acad. Sci. U.S.A.* **2000**, *98*, 2188−2193. (b) Garcia, A. E.; Sanbonmatsu K. Y. *J. Am. Chem. Soc.* **2002**, *99*, 2782−2787.

(58) McGregor, M. J.; Islam, S. I.; Sternberg, M. J. E. *J. Mol. Biol.* **1989**, *198*, 295−310.

(59) Rizo, J.; Blanco, F. J.; Kobe, B.; Bruch, M. D.; Gierasch, L. M.; *Biochemistry* **1993**, *32*, 4881−4894.

(60) Jimenez, M. A.; Blanco, F. J.; Rico, M.; Santoro, J.; Herranz, J.; Nieto, J. L. *Eur. J. Biochem.* **1992**, *207*, 39−49.